IAC-19-C3.IP.6

HARDWARE ARCHITECTURE OF ELECTRICAL POWER SYSTEM FOR 3U HYPERSPECTRAL IMAGING CUBESAT

Nihal Singh[a]*, Nishant Raman, Joy Parikh, Varun Goradia

[a] *Birla Institute of Technology and Science(BITS)-Pilani, India, 333031, http://www.bits-pilani.ac.in/*
* Corresponding Author

Abstract

This paper discusses the hardware architecture of the Electrical Power System (EPS) of a 3U CubeSat along with a fully functioning Simulink model of the same. This nanosatellite features a hyperspectral camera as its primary payload and a Field Programmable Gate Array (FPGA) as its secondary payload. Based on different power requirements of subsystems in various modes of operation of the nanosatellite, it was identified that the "Sun pointing with Image Compression mode" requires the maximum power of 9562.026mW. To satisfy the power requirements of all the components, the optimal solar panel configuration is chosen with solar cells placed on five out of six faces of the nanosatellite. The values for the inductor and capacitor in the boost converter are determined such that the output has minimum ripple magnitude and operates predominantly in Continuous Conduction Mode (CCM). Perturb and Observe (P&O) Algorithm for MPP tracking has been successfully tested using MATLAB, and the range of duty cycle was maintained within the desired range of 0.3 to 0.8 for various modes of operation. Sufficient power generation from the PV arrays has been verified through simulations by varying temperature and irradiance values expected in orbit. Batteries and their configuration were chosen such that the worst-case power requirements can be handled, and the ideal performance of the EPS for these power requirements was verified in Simulink. The selection and design of the various components and parts of the EPS are also mentioned in detail.

Keywords: EPS; Solar Cell; Boost Converter; MPPT; Li-Ion Batteries; OCPC

Acronyms/Abbreviations
EPS: Electrical Power System
MPPT: Maximum Power Point Tracking
FPGA: Field Programmable Gate Array
CCCV: Constant-Current Constant-Voltage
P&O: Perturb and Observe
OCPC: Overcurrent Protection Circuitry
CCM: Continuous Conduction Mode
DCM: Discontinuous Conduction Mode
SOC: State of Charge

1. Introduction

The Electrical Power System (EPS) is one of the six subsystems of a nanosatellite. In this paper, the EPS introduced is explicitly designed for a 3U CubeSat meant for hyperspectral imagery. EPS is the first subsystem to be turned on after deployment into the orbit and is essential for the operation of other subsystems. The nanosatellite depends on the EPS for power generation, power storage, and power transmission/distribution. The hyperspectral camera and the FPGA both pose harsh power constraints on a nanosatellite with limited power generation capabilities and battery capacity. It is for this reason that the EPS requires an efficient and resilient hardware architecture.

The Photovoltaic Arrays are connected through blocking diodes to the DC/DC boost converter implementing MPPT algorithms and control. The stepped-up voltage is then applied across the Lithium-Ion batteries, which are charged by the CCCV charging method. Batteries are connected in a 2S-2P(2 series-2 parallel) configuration across the output of the boost converter with the battery protection circuitry implementing overcharge as well as overcurrent

protection. Sensors interfaced with the microcontroller measures SOC of the batteries, the voltage across the batteries, and the current into the battery combination. Also, the sensor values obtained are used for battery charging control, satellite housekeeping data, and as parameters for switching between the modes of operation. A bus connected across the batteries leads to two Buck converters, which step down the battery voltage to 3.3V and 5V. These two buses provide power to the various subsystems of the satellite and have been successfully tested and implemented on both hardware and software. EPS also implements noise filtering and overcurrent protection circuitry for each subsystem.

2. Power Budget

The power budget of the nanosatellite describes the power consumption of the various components of the satellite and also assigns mode wise power consumption. The most power-intensive components on the nanosatellite are the Field-Programmable Gate Array (FPGA), the camera, reaction wheels, sun sensors, and the magnetorquer rod. Based on the power requirements of the components, it was identified that the "Sun pointing with Image Compression mode" [1] requires the maximum power of 9562.026mW. The power requirements of FPGA and the camera used are 7900mW and 1600mW, respectively. While the camera is needed to capture the hyperspectral image, the FPGA would be needed to run custom compression algorithms. The tasks carried out by both these power-intensive payloads are very crucial to the final aim of capturing the image and transmitting it to the ground station; therefore, it is crucial that these payloads are supplied sufficient power.

The power budget of the nanosatellite categorizes modes as being feasible or infeasible to enter into, based on the power generated and consumed during that mode's operation. The power that can be supplied to the subsystems during any mode is dependent on the state of charge of the batteries and the power generated by the solar panels, which is, in turn, dependent on the irradiation and temperature values.

In the MATLAB model, the various modes of operation of the nanosatellite have been modeled by setting loads of subsystems corresponding to the components which are operational in that mode.

3. Power Generation

Multi-junction solar cells were chosen to generate power on the nanosatellite as they have higher efficiencies, typically around 30% efficiency. The solar cells considered for this nanosatellite are the Azur Space Triple Junction 3G30C-Advanced Solar Cells. The solar cell of type A is a single cell with a V_{oc} value of 2.7 V and an I_{sc} value of 520.2mA. Each cell of type B has two solar cells of type A connected in parallel within it. Thus, both cell types A and B have V_{oc} as 2.7 V, whereas cell type B has approximately double the I_{sc} (1041 mA) as cell type A.

Solar panel configuration planned to be used in the nanosatellite is represented in Fig.1.
Following are the dimensions of the solar cells used:
Two adjacent large sides have 2 80x80 mm^2 cells and 3 40x80 mm^2 cells each (Area = 211.26 cm^2).
Two adjacent large sides have 1 80x80 mm^2 cells and 4 40x80 mm^2 cells each (Area = 181.08 cm^2).
The small side has 2 40x80 mm^2 cells (Area = 60.36 cm^2).

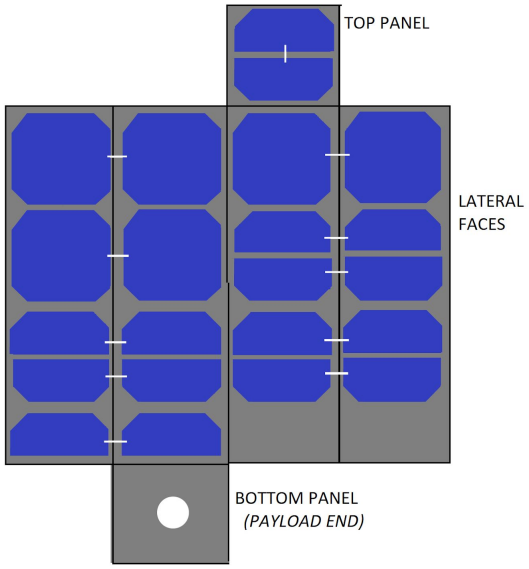

Fig.1. Solar panel Configuration

Thus, including both type A and type B cells, there are a total of 22 solar cells on five surfaces of the

nanosatellite, with one face having the camera assembly mounted. In compliance with telemetry requirements for antennas, some area on the two adjacent surfaces was left uncovered by solar cells.

When observing the I-V characteristics of a solar cell, it should be noted that the primary dependence of the Voc value is on the temperature, while the primary dependence of the Isc value is on the irradiance. The given solar cell architecture represents three parallel strings of type B solar cells in parallel with eight parallel strings of type A solar cells. Each string consists of two series-connected solar cells of the respective type.

When connected in series, the current through the solar cells is equal, while the voltage across each solar cell will vary depending on the temperature and irradiation values for the cell. It can thus be concluded that when solar cells are series-connected, they should be similarly illuminated so that the current output is the same for both of them. It is for this reason that solar cells on adjacent sides of the nanosatellite are connected in series.

While connecting solar cells in parallel, the current flow will be independently determined for each cell. In the parallel combination, the voltage across all branches will be equal; however, the cells will slightly differ in the voltage required across them to provide maximum power output. This is due to the shift in the I-V graph of the cell occurring as a result of the different irradiation on it. By having control of the voltage that can be forced across the combination of solar cell strings, the voltage can be set so as to maximize the input power from the solar cell combination.

4. DC-DC Converters and Maximum Power Point Tracking

As the batteries will always remain between 7.8-8.4 volts for a depth of discharge of 15%, the battery supply lines will also reflect this unregulated voltage. However, other components and subsystems onboard the nanosatellite require a steady power supply at either 5V or 3.3V. Therefore, a buck converter is needed to decrease and maintain the voltage to supply the two different voltage buses. For the purpose of the voltage step down, the LM2596 IC is used, which is available for 3.3V and 5V.

Based on the guidelines provided in the LM2596 datasheet, the inductor, output capacitor, and the input capacitor were selected for circuit design. Due to the low load current and high input voltage, a high inductance value was chosen. Due to the expected temperature variations, the input capacitor was chosen with a high RMS rating to drive high input current, and an output capacitor with low equivalent series resistance (ESR) was chosen to stabilize the output. The output voltage tolerance was experimentally found to be within 4%, as mentioned in the datasheet.

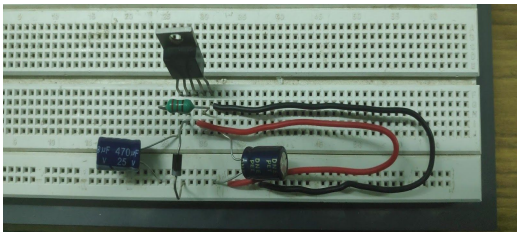

Fig.2. Buck Converter Circuit

The voltage obtained across the PV panel is less than the voltage needed across the batteries for charging purposes. It is for this reason that a Boost converter is used to step up the DC voltage output of the solar cells to meet the optimal voltage requirement for charging the battery combination. This DC-DC converter needs to be designed to step up the voltage from around 4.8V to above 7.2V while also implementing MPPT.

4.1 Circuit Implementation of Boost Converter

4.1.1 Introduction

To step up the voltage, a successful design of a boost converter was implemented from scratch, as shown in Fig 2. In order to successfully design a boost converter, the parameters need to be set appropriately in order to ensure that the output power requirements are met, variations are minimized while also ensuring that the converter does not enter discontinuous conduction mode (DCM), thereby providing a reliable step up functionality.

4.1.2 Modes of Operation

In continuous conduction mode (CCM), there is an approximate relation between the input and output voltage, given by $V\,in = (1 - D)V\,out$. For all practical purposes, it is desired that the converter always operates in CCM. The boost converter enters into DCM only when the ripple on the inductor current is large enough to cause the polarity of the MOSFET or diode to

change. For DCM, the relation between input and output voltage is given by $\frac{Vo}{Vi} = 1 + \frac{ViD^2T}{2LIo}$, and hence the output voltage depends upon the time period, inductance value, and output current. In DCM, energy discharges faster, which makes the peak current in the diode higher when compared to CCM. With a higher current, operating losses increase. There are three intervals in one cycle of DCM, unlike two in CCM, and the additional interval begins when the energy in the inductor is depleted and terminates at the end of the switching period as the switch turns ON. These time interval needs to be taken into consideration while determining the effective duty cycle.

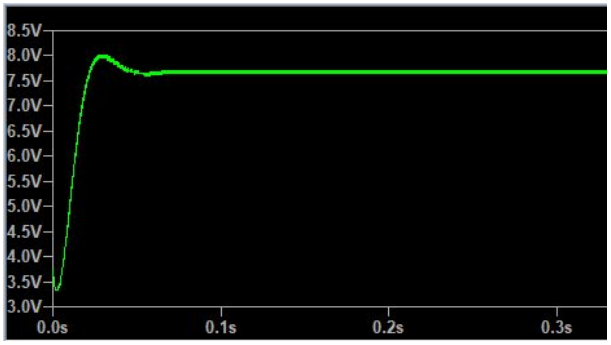

Fig.3. LTSpice Model of Boost Converter

$\frac{2L}{RT} > D(1-D)^2$ is the inequality that should be obeyed to disallow the converter from entering into DCM. Although DCM is capable of providing a good gain (Vout/Vin), it is not preferred over CCM due to high dependency on the above parameters. Apart from this, there are more overall losses in DCM operation, and the output gets affected by ringing and noise generation.

4.1.3 Component Value Realization

Based on the above information, the value of inductance was chosen to minimize the probability of entering into DCM while ensuring an ideal output voltage[2]. Experimentally, the current was found to fluctuate between 0.625 and 2.97A across different modes of operation with different power demands, for which corresponding L and C values were found to be 8.45 µH and 15.475 µF. It was found that the loads posed by the subsystems were quite low in value, and the consequent increase in the output current demanded from the boost converter can cause the converter to shift into DCM operation. DCM operation is not desirable as mentioned above, and hence to avoid it, the acceptable variations in the inductor current have to be increased to accommodate the large current variation between different modes as mentioned above. The increase in variation is a compromise acceptable in order to have a successful CCM operation. Earlier the acceptable Δi_L was kept at 10%, which is the accepted standard, but now due to new requirements, it was changed to around 60%.

4.1.4 Output Noise Analysis and Reduction

While the mode of operation of the converter (DCM/CCM) remains independent of the capacitance value, the amount of noise reduction in the output can be set by altering this value. Experimental results validated the same, as variation in capacitance value didn't change output voltage or the likeliness of the converter entering DCM. However, it was observed that there was a reduction in the ripples observed as the capacitance value was increased. A small-signal model of Boost Converter was considered to explore the effect of noise at the output[3]. Equation (1) governs the small signal variations, and after calculations, it was determined that the effect of noise was found to be negligible in the already closed loop boost converter implementation.

$$\begin{bmatrix} L\frac{di_l(t)}{dt} \\ C\frac{dV(t)}{dt} \end{bmatrix} = \begin{bmatrix} 0 & -D' \\ D' & -\frac{1}{R} \end{bmatrix} \begin{bmatrix} i_l(t) \\ V(t) \end{bmatrix} + \begin{bmatrix} 1 \\ 0 \end{bmatrix} V_g(t) \quad (1)$$

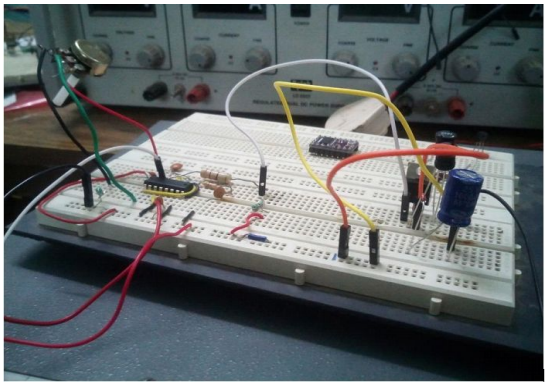

Fig.4. Boost Converter

4.1.5 MOSFET Model Selection

Based on the experimental analysis of MOSFETs as switches in boost converter circuits, it was observed that

self-heating in the MOSFET results in an increase in the device resistance. Apart from this, it was noted that the converter output voltage is an increasing function of load resistance in practical applications. It was also seen that the output voltage was a decreasing function of the frequency, which essentially places an upper limit on the switching speed of the MOSFET. Another upper limit on frequency is set by the fact that the device temperature increases with frequency. For high efficiency, it was also noted that an upper limit for the duty cycle needs to be set at 0.8 to prevent a rapid decline in the efficiency of the converter.

For the operating specifications of this paper, the best-suited MOSFET model for software simulation and analysis was identified as the Electrothermal model[4]. The electrothermal model of a MOSFET gives the best results for a PWM frequency of around 100khz, which is what this converter aims to operate at for ideal efficiency and high output. The electrothermal model of MOSFET was chosen over the hybrid model as it works almost equally well with PWM frequency less than 150 kHz, and at these lower frequencies of operation, the inertia of the MOSFET does not play a significant role in MOSFET selection.

4.1.6 MPPT

If the boost converter is designed from scratch without the use of any IC, maximum power point tracking needs to be implemented using code that will be run on the EPS microcontroller. The aim of maximum power point tracking is to extract maximum available power from the combination of solar cells under the prevalent conditions. The voltage corresponding to the maximum power output of the PV module is called the peak power voltage. Since the voltage at the output of the boost converter is almost constant over the small duration of time that the MPPT algorithm takes to operate, the best way to maximize current into the battery is to maximize the power input to the boost converter from the PV array. This ensues from the fact that power must be conserved at input and output of the boost converter.

There are three main MPP tracking algorithms for a PV array. There is the Perturb and Observe algorithm (P&O), Incremental conductance method, and Constant voltage method. The incremental conductance method is very similar to the P&O method except that in P&O, additional computation of power from voltage and current is required. However, it was seen that for the expected fluctuation in irradiance and temperature, P&O performs the best. The P&O algorithm varies the duty cycle of the PWM signal to the MOSFET of the boost converter based on the slope of the P-V graph, thereby changing the duration of operation of each of the two modes of the boost converter. Finally, the standard P&O algorithm was selected over fuzzy logic P&O as the added accuracy and speed provided by the latter were not worth the additional computational overhead.

4.2 SPV1040 as a Boost Converter

Apart from designing a boost converter, the SPV1040 IC was also tested as an integrated boost converter and battery charger that implements the MPPT algorithm. For connecting solar panels to SPV, the first option available is to connect an SPV to each solar cell, resulting in 22 SPVs. This occupies a large amount of area and adds a lot of weight to the satellite, and hence a more optimized architecture was needed.

Fig.5. SPV Boost Converter & Battery Charger

As it is intended to charge a combination of lithium-ion batteries with a total voltage of 8.4V across them, two SPVs are required to be connected to the combination, and each one should have a maximum output voltage of 4.2V. Given that the output of the solar cells is 2.7V, solar cells can never be connected in series to a single charger for the proposed solar cell architecture. This would result in the input voltage being larger than the output voltage, which is highly undesirable for any boost converter (Even two solar cells connected in series will result in an input voltage of 5.4V, which exceeds the desired output). Thus, a method was proposed in which the solar cells on

opposite faces of the nanosatellite are connected in parallel to a single SPV. The SPV will then set the voltage across the solar cells to ensure that maximum power is inputted from the solar cells. Using these connections a total of 6 SPVs are obtained on the side surfaces, excluding the two solar cells of type A connected in series on two of the sides and the top surface of the nanosatellite. These remaining solar cells will require an additional 2 SPVs, resulting in a total of 8 SPVs.

Hence, for implementation of a boost converter using SPV IC, a total of 8 SPVs will be needed based on the chosen PV array and battery configuration.

5. Power Storage → Batteries and Charger

To store excess power generated by solar panels, and supply it to the various loads when the solar power generated is insufficient, batteries are needed. The Lithium-Ion batteries chosen and tested are the rechargeable Panasonic NCR18650B cells with a typical capacity of 3350 mAh and a nominal voltage of 3.6V. Li-Ion batteries were chosen as they have a high energy density, and unlike NiCd or NiMH batteries, they do not exhibit the memory effect. This increases the lifetime and the total number of charging and discharging cycles possible. In order to charge the batteries efficiently and safely, appropriate battery protection circuitry is used, and charging of the batteries is done using a constant-current constant-voltage charger (CCCV). The CCCV charger also helps in improving the lifetime of the battery over several charging cycles.

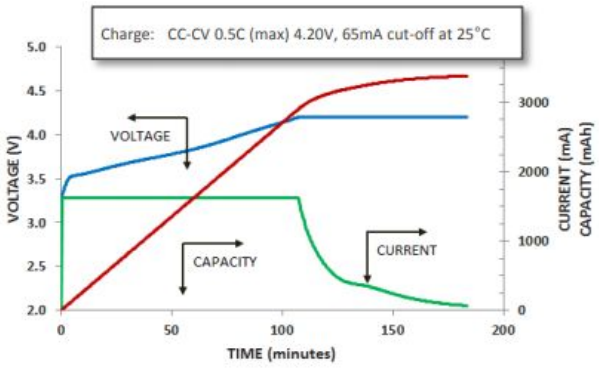

Fig.6. Charging of NCR18650 battery

Small differences in self-discharge rates and parasitic loads among series-connected cells result in unequal cell voltages. It is for this reason that it was decided to balance the battery cells by connecting the two parallel branches such that the voltage across the top battery and bottom battery in a branch is equal to that of the corresponding battery in the other branch. This helps to prevent the divergence of cell voltages within a battery. For battery charging, two ICs have been tested, the BQ2057w and the SPV1040.

The BQ2057w battery charger has an AutoComp feature for fast charging, which would prove extremely beneficial to the subsystem. This battery charger implements charging in constant current mode and constant voltage mode with high accuracy, while also having an initial preconditioning phase which supplies 10% of the desired current. Furthermore, this IC also has an inbuilt over-temperature protection circuitry ensuring its reliability.

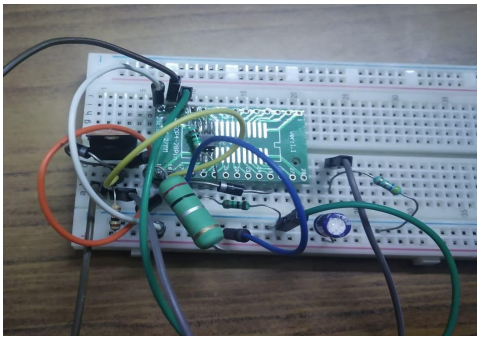

Fig.7. BQ2057w Circuit Implementation

The SPV1040 previously tested for its inbuilt MPPT algorithm and voltage boosting capability also has an integrated battery charging circuitry. This IC removes the need for a separate Boost Converter and implementation of an MPPT algorithm, thereby simplifying the overall architecture. The SPV1040 also has the feature of reverse polarity protection and over-temperature control. This IC works in six modes-shutdown mode, soft-start mode, start-up mode, MPPT mode, Burst mode, and sleep-in mode, thereby providing a wide range of functionality. Apart from this, the IC also consumes less power and has been previously used in KufaSat and NTNU's nanosatellite.

6.Housekeeping Data and Sensors

There are several sensors interfaced with the EPS to record housekeeping data, control battery charging,

track maximum power point of the PV array, and determine values of parameters to decide the switching between modes of operation.

For temperature and current sensing, the LM75 IC and the INA219 IC are used respectively. It was decided to have a coulomb counter interfaced with EPS to calculate the SOC of the battery. Coulomb counter is used to prevent multiple interrupts to the microcontroller and is far more efficient and accurate than using a current sensor and integrating the values over a period of time on the MCU. It is also possible to set the frequency of interrupts of the coulomb counter by setting the Rsense value.

7.OCPC

Overcurrent protection circuitry (OCPC) is needed to stop or limit the current flow to a particular subsystem during the event of a failure. This need for current regulation is present to minimize the likeliness of any possible damage and associated power loss. Every subsystem requires an OCPC, and this circuit should be able to protect the subsystem in case of any fault or single event latch-up. Currently, the IC used to implement OCPC is TPS2553-1. It is a current latch off circuit that offers a programmable current-limit threshold between 75 mA and 1.7 A by the use of an external resistor.

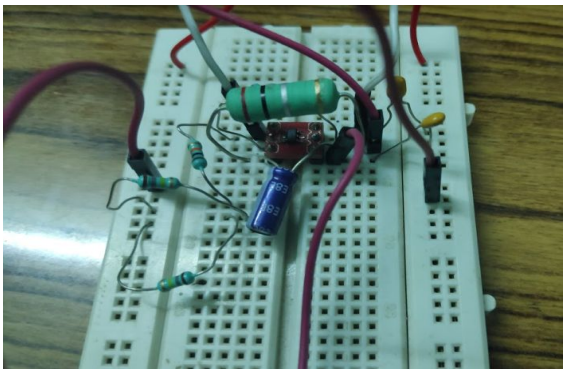

Fig.8. OCPC

Initially, the TPS2553 IC was used, but this IC was meant for current limiting rather than for current latch off. Due to the better performance of the latch-off OCPC, that IC was chosen for implementation instead. The EPS microcontroller (MCU) will be connected to the IC such that a fault signal will give the MCU information of an overcurrent event. Along with that, the microcontroller will control the enable signal. To have the ability to remove an SEL quickly, TPS2553-1 will also be configured in auto-retry mode. When the fault signal is asserted, the switch will be disabled, and depending on the RC time constant of the Cretry and Rretry; the delay will be determined before re-enabling the switch.

For OCPC, a comparator circuit was also developed using MOSFET - comparator configuration, which provided satisfactory results. The operational amplifier LM358SN was used for this testing. The circuit had a lower limit for current limiting due to input offset voltage of the comparator, which was calculated and experimentally verified to be 80mA. The response time for this circuit was 5s, and for better results, the circuit using comparator AD8564 will be tested to improve the response time to 7ns.

8.Filters

The switching of loads at the output of the buck converter may cause noise in the supply bus. Filters are used to reduce this noise and remove the high-frequency content to give approximately a constant DC output. Based on the response and the stability of the system, a second-order low pass filter consisting of an inductor and capacitor was chosen. The main reason for opting for a second order LPF over a first-order LPF was because the former has double the stopband roll-off of the latter, thereby having a steeper transfer function and better filtering capability.

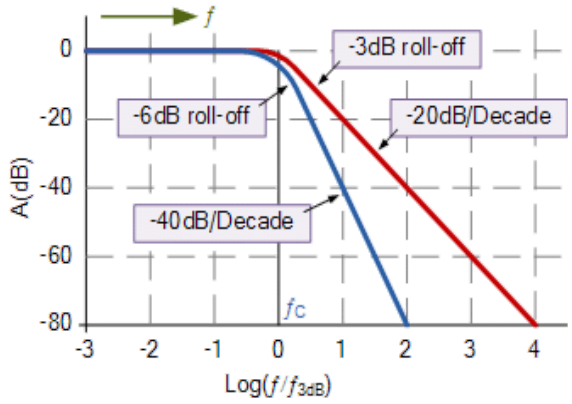

Fig.9. Filter

As not using filters may result in fluctuations in other subsystems as well, it was decided to connect a filter before every subsystem.

9.Simulink Model

The MATLAB model of the Electrical Power System is shown in Fig.10. In this model, a model of a PV array was used as input based on the specified solar cell configuration, consisting of 11 total parallel strings of two cells each. While three of these parallel strings consist of cells of type A, the remaining eight strings consist of cells of type B.

The specifications of each cell in the MATLAB model is in accordance with the datasheet of the Azure solar cells that are intended for use on the nanosatellite. The PV panel has input variables of irradiance and temperature, which is set based on the estimated values of these corresponding variables in orbit. These values are fed as input parameters to the PV panel to obtain the behavior of the model for a vast and dynamic range of inputs. Following the PV panel, there is a blocking diode placed to ensure unidirectional flow of current from the PV panel to the input of the boost converter.

The model of the boost converter is made in accordance with the values calculated in the DC-DC converters section. However, the value of capacitance was slightly increased in order to provide a more stable functionality. In the model for the boost converter, a MATLAB block for the P&O algorithm was inserted, where it is decided at regular intervals whether to increase or decrease the duty cycle by a preset amount. The MATLAB function is representative of the microcontroller's functionality, which would be running the algorithm onboard in real-time. The output of this block is fed to the PWM generator, which in turn drives the MOSFET. This simulation was also tested by using a Spice model of the boost converter directly into Simulink.

At the output of the boost converter, a diode was connected, which leads to the battery combination containing four batteries connected in two strings with two batteries in each string with cell balancing implemented. Across the output of the batteries, a capacitor was placed to smoothen out the rapid fluctuations in the current flowing into the battery combination. Across the battery supply lines, two buck converter models were placed in parallel, stepping down the battery voltage to 5V and 3.3V respectively to supply power to the various components on the nanosatellite.

In this section, a deep dive will be done on the 'Image taking mode' of operation of the nanosatellite. This mode is chosen for analysis as it is the only mode wherein components are connected across both 3.3V and 5V bus. As only one mode is being simulated, the bus fluctuations caused by load switching are nonexistent, and hence the filters have been neglected from the model for this simulation. Based on the chosen mode of operation, each subsystem has specific components consuming power and operating across a specific voltage bus.

For the Telemetry subsystem, the components that require power in this mode are; OOK Modulator (19.06mW), RF Switch (0.066mW), High Power Amplifier (185mW), and microcontroller (0.9mW). When modeled as an equivalent impedance across the 5V bus, it is seen that the impedance value is 121.94 ohms. For the Attitude Determination and Control subsystem, the components that require power in this mode are; Reaction Wheels (2550mW), Sun Sensor (750mW), and other sensors (50mW). When modeled as an equivalent impedance across the 5V bus, it is seen that the impedance value is 7.46 ohms. For the On-Board Computer subsystem, only the microcontroller needs power in this mode. The microcontroller has an equivalent impedance of 62.5 ohms. The primary payload (camera) is connected across the 3.3V bus and requires 1600mW of power to operate. When modeled as an equivalent impedance across the 3.3V bus, it has an equivalent impedance value of 6.8 ohms.

When this mode was simulated, it was seen that the duty cycle of the boost converter settles at a value 0.494 within seconds when a constant temperature and irradiance of 25 degrees and 1350 W/m2 is set. For these fixed input parameters and loads, the battery combination had a rise of 0.5% SOC within 80 seconds of simulation. The initial SOC of the battery was set to 85%, and at 85.5% SOC, the duty cycle was constant with the voltage across the PV array set at 4.626V. While the duty cycle of the boost converter took several seconds to become constant for constant input parameters, the buck converter took just a few milliseconds. At the maximum power point, the power generated by the solar cell combination with these inputs was 19.73W. The duty cycle of the 5V and 3.3V buck converters settled at 0.6703 and 0.4698, respectively.

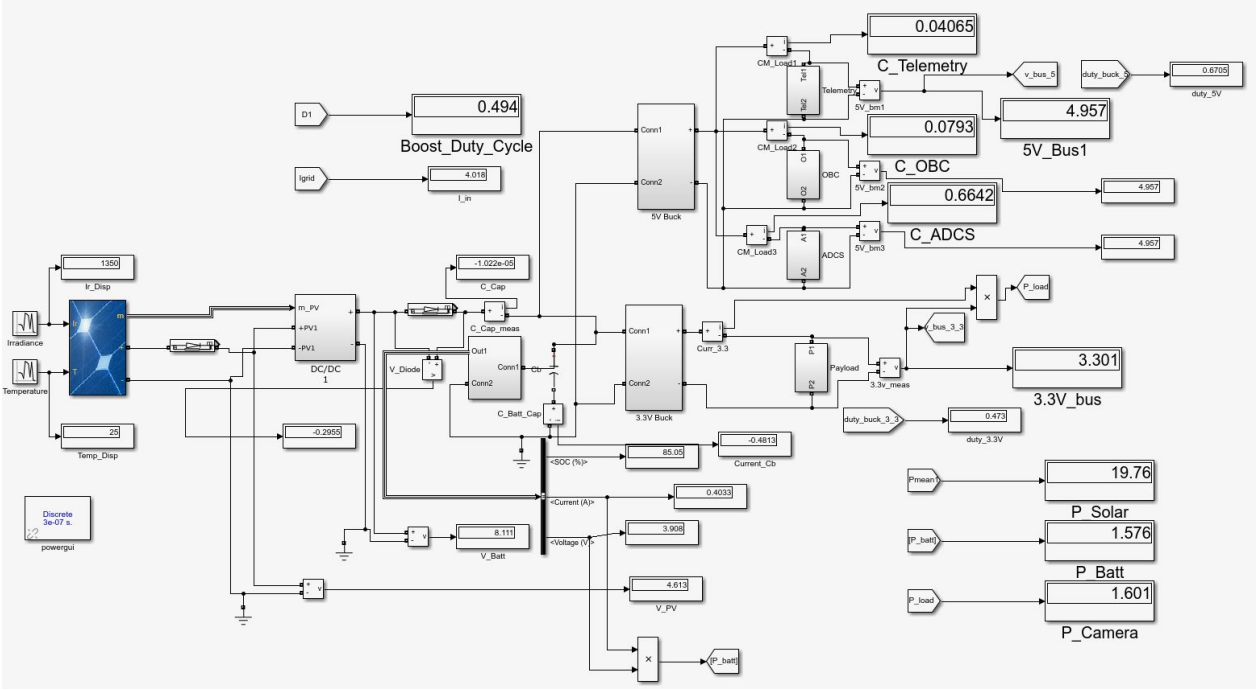

Fig.10. Simulink Model

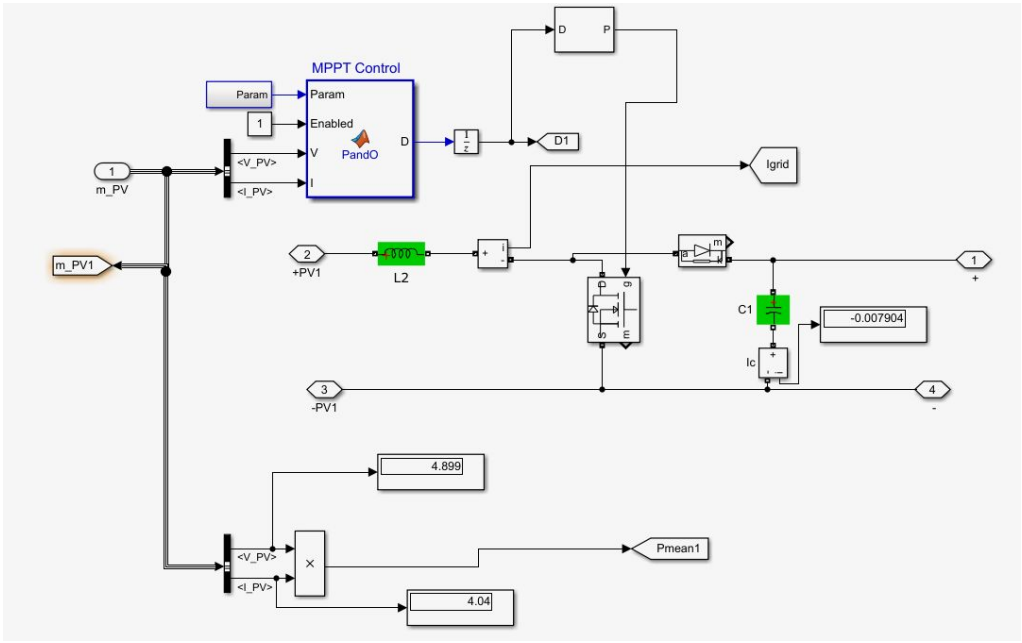

Fig.11. Boost Converter Model

10. Conclusions

Designing an electrical power system for a nanosatellite has many critical elements, both in the architecture and component selection. A basic layout of the EPS has been discussed in the paper, with emphasis on the design of each hardware block. While a full hardware implementation remains to be done for some components, a comprehensive simulation model of the proposed hardware architecture has been designed and tested on the Simulink software. While hardware realization is the final goal, a software model incorporating updates in research and design is an essential bridge between the former and the proposed theoretical architecture. The successful implementation of a Simulink model is a preliminary step that serves as a proof of concept and a basis for actual hardware development. A software implementation is also critical as rigorous testing conditions can be simulated, and the design's resilience can be put to extreme tests, which can be difficult to introduce on actual hardware. With this, it is seen that the satellite is sustainable, and the mission is achievable.

References

Reference to a conference/congress paper:

[1] Rutwik Jain, Shubham Sharma, Modes of Operation for a 3U CubeSat with Hyperspectral Imaging Payload, IAC-18-D1.2.8, 69th International Astronautical Congress, Germany, Bremen, 2018, 1 – 5 October.

[3] M. Sai Krishna Reddy, Ch. Kalyani, M. Uthra and D. Elangovan, A Small Signal Analysis of DC-DC Boost Converter, Indian Journal of Science and Technology, Vol 8(S2), 1-6, January 2015

[4] Krzysztof Gorecki, Janusz Zarebski, Influence of MOSFET model form on boost converter characteristics at the steady state, 2009 MIXDES-16th International Conference Mixed Design of Integrated Circuits & Systems, IEEE, 10939978, 25-27 June 2009.

Reference to a report:

[2] Lars Alminde, Gert K. Andersen, Power Supply for the AAU Cubesat, University of Aalborg, 01GR509, December 20, 2001.